The fracture of a climbing rope: a phenomenological approach

Sept. 2018

Ulrich Leuthäusser

For the fracture process of a climbing rope, two mechanisms are responsible: plastic deformation and local damage of the contact zone between rope and anchor. These mechanisms are described by two analytical models represented by nonlinear difference equations.

The plastic deformation equation can be linked to a catastrophe-theoretical model. From the equation describing local damage accumulation, the Palmgren-Miner rule can be derived.

The used energy-based approach allows the combination of these models and thus the calculation of the number of falls to failure as a function of the ratio of fall energy/energy storage capacity.

The behaviour of climbing ropes tested by subsequent UIAA falls can be quantitatively explained by these models.

V.0.9

 © 2018 Ulrich Leuthäusser

1. Introduction

Modelling material failure and damage is an extremely important and intensely investigated field. Because of its interdisciplinary character covering disciplines like elasticity and plasticity theory, as well as statistical physics and probability theory, one is confronted with interesting and challenging tasks. Comprehensive overviews are abundant[1,2,3].
To date, minimal work[4] has been done on climbing ropes. Fiber bundle models,[3,5] which might be possible candidates for a climbing rope, are not completely appropriate because their parallel structure does not reflect the complicated twisted construction of a climbing rope.
In this paper, the accumulation of damage in a climbing rope by successive dynamic impacts under UIAA standard conditions[6] and its subsequent fracture are investigated.
Its central goal is to develop models for the damage mechanisms which diminish the energy storage capacity of the rope. These relatively simple models can be treated analytically in order to obtain transparent closed form solutions. In a second step, the theoretical results will be applied to experimental force–deformation curves of sequential UIAA standard falls[7] until the rope breaks. In detail, several intriguing questions have to be answered. How is it possible that the measured spring constant of a climbing rope increases with increasing number of falls, although damage, as a gradual weakening of the material, usually leads to a softening of the spring constant? Climbing ropes differ widely in their number of falls to failure. Is it possible to obtain a relation between the applied stress level and the number of falls to failure like the stress-cycle (SN) curves for other materials, which is approximately universal for all climbing ropes? Furthermore, polyamid (nylon), the material which ropes are made from, suddenly shows plastic behaviour when a certain yield stress is exceeded. The question arises whether this elastic-plastic transition can be detected.
The structure of the paper is as follows. After this introduction, the plastic deformation of a rope is investigated in section 2. First, an appropriate elastic force representing the polymer properties is introduced. It enters the equation of motion from which the maximum impact force of a fall can be calculated. If this force is larger than a certain threshold, it initiates irreversible plastic flow. Using a simple hardening rule, the plastic flow is described by a nonlinear difference equation. At a critical stress, this equation shows a sudden transition from a stable solution of a finite deformation to an unstable solution representing fracture. Plastic deformation of the rope, however, is not sufficient to explain its fracture. Therefore, in section 3, a second fracture mechanism is analyzed. While the first damage mechanism of overstretching is of global nature and affects the entire rope mainly by reducing its maximum possible elastic deformation, the second damage comes from the contact of the rope with an anchor point. In this contact zone, large stress concentrations lead to local damage of the rope, mainly by reducing its cross section. This damage is discussed in terms of a statistical Weibull failure model.
In section 4, the two failure mechanisms are combined. This is possible, because they both reduce the energy storage capacity of the rope. Fracture occurs when the fall energy exceeds this capacity. This condition leads to an explicit expression for the critical number of falls to failure as a function of the fall energy. Furthermore, a connection to the known Palmgren-Miner rule is made showing the universality of the applied approach. Because of the probabilistic nature of the damage process, the number of falls to failure fluctuates. A formula for these fluctuations is also presented at the end of this section.
In section 5, the theoretical results from the former sections are compared with fall experiments. The applicability of the presented methods is not restricted to climbing ropes. The choice of a climbing rope is based on personal interest and the availability of good measurements. Other applications would include ropes for speleo, canyoning and sailing.

 © 2018 Ulrich Leuthäusser

2. Homogeneous plastic deformation of the rope

Climbing ropes are made of polyamid. This polymer shows yield behaviour[8], i.e. for stresses above a certain yield stress a permanent plastic deformation remains. It reduces the maximum elastic deformation and thus the strain energy capacity of the rope. Below the yield stress, polyamid deforms elastically and completely returns to its initial state.
Apparently, plastic and elastic deformations of a material have to be discussed together.
The basic elastic properties of polymer fibers can be described by a statistical mechanics model consisting of a chain of freely orientable independent segments[9]. From that model, an elastic force F^{La} is obtained as given by the inverse of the Langevin function $La(x) = \coth(x) - 1/x$ which has no analytical representation.

Both F^{La} and its corresponding strain energy U diverge at the maximum possible elastic deformation L^e, i.e. unlimited energy can be transferred to the chain. But to describe the fracture of the polymer chain, a finite maximum energy content is necessary. The following elastic force, shown in Eq. (1)

$$F(x,L^e) = a_1 \frac{x}{L^e} + a_3\left(\frac{x}{L^e}\right)^3 \cong \frac{a_1}{3} La\left(\frac{x}{L^e}\right)^{-1} \qquad \textbf{(1)}$$

is similar to F^{La}, but at L^e, the force F has a maximum value of $F^{max} = a_1 + a_3$ with a maximum strain energy $U = 1/2\, L^e\left(a_1 + a_3/2\right)$ instead of a singularity. Note that F, just as its origin F^{La}, is only a function of the relative elongation x/L^e and an odd function of this argument without a quadratic term in x/L^e. Such a term would lead to an unstable equilibrium at x = 0 in the underlying potential function.
For the later discussion, it is useful to treat the power law parts of F separately and denote them as $F^m = a_m (x/L^e)^m$. For a dynamic load experiment with a falling mass of energy U^{fall}, the maximum $\hat{F}^m$ are related to U^{fall} by the relation $\frac{\hat{F}^m}{(F^m)^{max}} = \left(\frac{U^{fall}}{U^m}\right)^{\frac{m}{m+1}}$ with the maximum possible strain energy $U^m = \frac{a_m L^e}{m+1}$ and the corresponding maximum force $(F^m)^{max} = a_m$.

The parameter $\alpha = a_3/a_1$ depends on the method how $F^{La} = \frac{a_1}{3} La\left(\frac{x}{L^e}\right)^{-1}$ is approximated. From the Taylor expansion of F^{La} valid for small x, one finds $\alpha = 3/5$, whereas minimization of the quadratic error of $F - F^{La}$ in the large interval [0, 0.8L^e], yields a twice as large $\alpha \approx 4/3$ with a maximum relative error of 12% at 0.8L^e.
For x/L_e = 0.6, the contribution of the nonlinear part is already 30% of F. This strong nonlinear behaviour corresponds to the experimental force-deformation curves shown in Fig. 3.

For small elongations where Hooke's law is valid, the spring constant $k = a_1/L^e$ as the initial slope of the force-deformation curve can be read off. k is related to the elasticity modulus E by $k = EQ/L$, where Q is the cross section of the rope. L^e is therefore proportional to the initial unstretched rope length L. The maximum stretching capacity L^e/L, as the proportionality factor, is for polyamid between 1.5 and 1.55[10].

For a dynamic load experiment with a falling mass M of energy U^{fall}, the maximum $\hat{F}$ of the force $F(x,L^e) = a_1\left(x/L^e + \alpha\left(x/L^e\right)^3\right)$ from Eq. (1) is related to U^{fall} by Eq. (2)

$$\frac{\hat{F}}{F^{max}} = \frac{\hat{\sigma}}{\sigma^{max}} = \frac{1}{\sqrt{\alpha}}\frac{1}{1+\alpha}\sqrt{\sqrt{1+\alpha(2+\alpha)\frac{U^{fall}}{U}}-1}\cdot\sqrt{1+\alpha(2+\alpha)\frac{U^{fall}}{U}} \cong \left(\frac{U^{fall}}{U}\right)^{\frac{3}{4}} \qquad \textbf{(2)}$$

For $\alpha = 4/3$, the last term of Eq. (2) has a relative absolute error less than 4% for $U^{fall} \geq 0.2U$.
In the following, often the stress $\sigma = F/Q$ is used instead of the force F. Its maximum value σ^{max} is related to the maximum density of the energy storage capacity u^{max} by $\sigma^{max} = 4\frac{1+\alpha}{2+\alpha}\cdot u^{max}$ so that $\hat{\sigma}$ can be expressed completely in terms of energies.

Once F is determined, the elastic deformation $x_n(t)$ for each fall number $n = 1, 2, \ldots$ can be calculated by the following equation of motion

$$M\ddot{x}_n(t) - Mg = F\left(\frac{x_n(t)}{L_n^e}\right) \qquad \textbf{(3)}$$

where the L_n^e depend on n with L_1^e as the initial maximum elastic deformation before the first fall. Eq. (3) can be applied from the beginning of the fall up to the maximum F = $\hat{F}$. In that time interval, friction can be approximately neglected because stretching is an adiabatic process. This leads to delayed friction[11] and therefore the elastic F dominates. Only after the maximum, the force decreases at almost constant deformation, leading to strong dissipation and the hysteresis loops seen later in Figs. 3 and 4.

Next, for the investigation of the plastic deformation, we start with the following microscopic picture. The yield stress, as a threshold, indicates an activated process. That is, the polymeric units when stretched over that threshold, cross an energy barrier. When the external stress is released, they are trapped in a new potential, which corresponds to a configuration of unfolded polymer units without the possibility to return to their initial state. The new state has still macroscopic elastic properties, but with a smaller maximum elastic energy. The activated process is described by transition state theory of viscous flow. For low temperatures (which lead to an abrupt transition into the plastic state), an approximation in the following simple form is possible as shown in Eq. (4)

$$\Delta\varepsilon_1^p \equiv \varepsilon_1^p - \varepsilon_0^p = \begin{cases} \frac{1}{\eta}\left(\hat{\sigma}_1 - \sigma_0^y\right) & \hat{\sigma}_1 \geq \sigma_0^y \\ 0 & \hat{\sigma}_1 < \sigma_0^y \end{cases} \qquad \textbf{(4)}$$

where the plastic strain rate $\Delta\varepsilon_1^p$ after the first fall is proportional to the difference of the external maximum stress $\hat{\sigma}_1 \equiv \hat{\sigma}(L_1^e)$. σ_0^y is the yield stress in the first fall, which is a characteristic constant of the material used. The initial ε_0^p is zero and η is a viscosity parameter. The phenomenological Bingham model[12], as one of the basic models of plasticity, has exactly the same form as Eq. (4).

In the subsequent falls, the yield effect is increasingly smaller. Microscopically, many elastic units are already trapped in the unfolded state, and only larger stress leads to additional transitions of elastic units in the unfolded state. Macroscopically, this phenomenon is called strain hardening, which results in an increased spring constant and an increased resistance against stress, combined with an onset of plastic flow only for a stress larger than the already reached stress.

Therefore, it is assumed that the yield stress for the nth fall σ^y_{n-1} is given by the maximum stress of the preceding fall $\hat{\sigma}_{n-1}$. With this hardening rule, all $\Delta\varepsilon^p_n$ can be summed up with the result

$$\varepsilon^p_n = \frac{1}{\eta}\left(\hat{\sigma}_n - \sigma^y_0\right) \tag{5}$$

The complete plastic deformation depends only on the maximum stress $\hat{\sigma}_n$ that was exerted to the rope. Eq. (5) is independent of the specific order of the $\hat{\sigma}_n$, a descending order instead of an ascending one would lead to the same result. This is in agreement with the idea of an underlying activated process. In addition, this process predicts a linear temperature dependence of η which could be a test of the model. Furthermore, in order to combine elastic and plastic deformations, it is assumed that the plastic deformation reduces the maximum possible elastic deformation as follows

$$\frac{L^e_{n+1}}{L^e_1} = 1 - \varepsilon^p_n \,. \tag{6}$$

This relation is illustrated in Fig. 1.

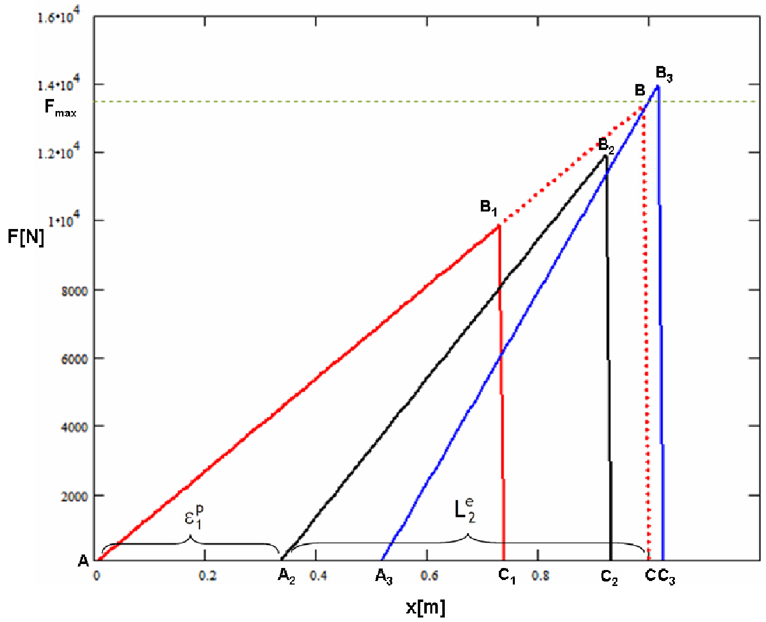

Figure 1. Illustration of the interaction of plastic and elastic deformation for a linear force.
The red curve represents the first fall and shows the force-deformation curve. The dotted line is its continuation up to the maximum possible force F^{max}. The area of this triangle ABC is the maximum initial energy capacity, the area AB_1C_1 represents the fall energy U^{fall}. Because the maximum of F at B_1 is larger than the yield force, plastic deformation sets in and leads to an $\varepsilon^p_1 \approx$ 0.35 and a smaller $L^e_2 \approx 0.65$ (compared to $L^e_1 = 1$) for the second fall which is represented by the black curve. The slope $F'_2(x)$ is steeper, i.e. the spring constant is larger, and the remaining energy content (area A_2BC) is reduced. The blue curve is the fall where fracture occurs. The maximum force F^{max} is exceeded because the fall energy (area $A_3B_3C_3$) is larger than the remaining elastic storage energy (triangle A_3BC).

 © 2018 Ulrich Leuthäusser

Eqs. (3) and (5), together with the last relation, completely describe the sequence of the plastic and elastic deformations and can be solved numerically in the following way. For the first fall n = 1, the solution of Eq. (3) with the initial L_1^e determines the maximal $\hat{F}(L_1^e) = Q\hat{\sigma}_1$. With $\hat{\sigma}_1$ the plastic deformation ε_1^p is calculated from Eq. (5) which leads to a new L_2^e because of Eq. (6). L_2^e enters again in Eq. (3) for the second fall, and so on.
It should be noted, that this sequential approach between elastic and plastic deformations is only correct if the plastic deformation completely occurs on the backward motion of the rope, but it begins shortly before the maximum of elastic deformation has been reached and leads to a flattening of the force.
With the relation $\hat{\sigma} \propto U^{3/4} \propto (L^e)^{3/4}$ from Eq. (2) together with Eq. (6), Eq. (5) can be written as a difference equation for ε_n^p alone. Introducing the dimensionless quantities $s_1 = \hat{\sigma}_1/\eta$ and $s_0 = \sigma_0^y/\eta$ one obtains Eq. (7)

$$\varepsilon_{n+1}^p = s_1\left(\frac{1}{1-\varepsilon_n^p}\right)^{\frac{3}{4}} - s_0 \quad \textbf{(7)}$$

This equation describes the dynamics of the elastic-plastic transition, as well as fracture beyond a critical stress.
To calculate its asymptotic behaviour, s_1 is considered as a function of ε_n^p in the steady state limit $n \to \infty$. A short calculation shows that s_1 has a maximum value $s_1^c = \frac{4}{7}\left(\frac{3}{7}\right)^{\frac{3}{4}}(1+s_0)^{\frac{7}{4}}$ at $(\varepsilon_\infty^p)^{max} = \frac{4-3s_0}{7}$ without real solutions for $s_1 > s_1^c$. Thus, when the maximum stress of the first fall $\hat{\sigma}_1$ reaches a critical stress $\hat{\sigma}_1^c = \eta s_1^c$, the behaviour of Eq. (7) suddenly switches from a stable solution to an unstable one, indicating fracture. Note that this transition does not depend on a threshold s_0>0. It is also possible for s_0=0.
For $s_1 \le s_1^c$, the ε_n^p converge to a finite ε_∞^p which cannot be calculated exactly. But ε_∞^p has an excellent approximation given by Eq. (8)

$$\frac{\varepsilon_\infty^p}{(\varepsilon_\infty^p)^{max}} = 1 - \sqrt{1 - \frac{s_1 - s_0}{s_1^c - s_0}} \quad \textbf{(8)}$$

with a relative error smaller than 3.2% in the complete interval $s_0 \le s_1 \le s_1^c$. The square root which appears in the asymptotic solution of Eq. (8) points to an underlying quadratic difference equation for ε_n^p of the form $\varepsilon_{n+1}^p = c_0 + c_1\varepsilon_n^p + c_2\left(\varepsilon_n^p\right)^2$. By the method of equating the coefficients, the c_i can be determined. This difference equation with the quadratic nonlinearity represents a fold catastrophe[13] as the simplest bifurcation in catastrophe theory.
In the stable case $s_1 \le s_1^c$, the asymptotic ε_∞^p as well as the $\varepsilon_1^p = s_1 - s_0$ of the first fall are known. Using these two values, ε_n^p can be interpolated by Eq. (9)

$$\varepsilon_n^p = \varepsilon_\infty^p\left(1 - \left(1 - \frac{s_1 - s_0}{\varepsilon_\infty^p}\right)^n\right) \quad \textbf{(9)}$$

with the same small error as the error of Eq. (8).

© 2018 Ulrich Leuthäusser

OW

Because the maximum energy storage capacity is proportional to L_n^e, Eq. (7) also determines the elastic energy content $U_{n+1}^e / U = 1 - \varepsilon_n^p$ as well as the final energy content $U_\infty^e / U = 1 - \varepsilon_\infty^p$. Assuming that the yield stress σ_0^y is mainly a property of the material and because of Eq. (2), U_∞^e / U can be expressed solely in terms of the ratio U^{fall} / U.
Finally, the described instability leading to fracture is not a nonlinear phenomenon. A linear force leads to an equation similar to Eq. (7) with an exponent ½ instead of ¾ also showing a divergent solution beyond a critical value of s_1.

σ-dW

3. Localized damage of the rope's contact zone with the anchor point

In the standard UIAA impact test, the rope runs over an anchor point where it is deflected approximately 180 degrees. This region between rope and anchor is called the contact zone, which is small compared to the total length of the rope. In this contact zone, the external σ induces an additional complicated field of compressive and shear stresses depending on the radius r of the anchor point.

Because the contact area between the rope and anchor point is approximately given by $Rr\pi$ (R is the radius of the rope), the local stress is given by $\sigma_{loc} \propto (F/rR)$ with the external force F from Eq. (1).
In a phenomenological analysis, the fracture process for a rope, which is exposed to an external stress, can be described by the widely used Weibull failure probability P_f. Using the forces F^m, introduced in the last section, it takes the following form

$$P_f(x) = 1 - P(x) = 1 - \exp\left(-\mu (x/L)^{m\lambda}\right) \qquad \textbf{(10)}$$

where μ is a damage parameter in which some parameters have been merged. In particular, it depends on the anchor radius r.
The smaller the r, the more the contact area is weakened by surface abrasion. This leads to a large μ and thus to large local damage, whereas for $r \to \infty$ the local damage disappears. The parameter λ can be estimated from contact mechanics. For some simple geometries[14], and in the linear case m=1, its value is approximately 2. Furthermore, the rope length $L \propto L^e$ instead of L^e has been used in Eq. (10).
Now consider a rope which has a contact zone with length L^A and a cross section Q^A. The undamaged rest of the rope is analogously described by L^B and Q^B as shown in Fig. 2.

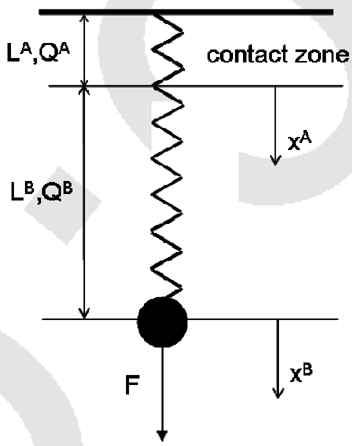

Figure 2. Illustration of the contact zone of length L^A,cross section Q^A and its deformation x^A. The undamaged part of the rope has the superscript B.

The total spring constant of the rope is given by $k = E Q^A Q^B / (Q^B L^A + Q^A L^B)$. For a smaller local cross section Q^A as the cross section Q of the undamaged rope, the relative change of k for $L^A << L^B \approx L$ is given by $\Delta k/k \approx L^A/L \cdot (Q^A - Q)/Q^A$. Thus, local damage leads only to a small negative change of k proportional to L^A/L . It cannot be detected by the force measurements because it is covered by the much larger global plastic stiffening.

Next, one has to determine which fraction of the fall energy U^{fall} is allocated to the contact zone. Energy conservation at maximum deformation, where the kinetic energy of the fall mass is zero, has to take into account the elastic energy contribution U^A of the contact zone and U^B of the rest of the rope as shown in Eq. (11)

$$U^{fall} = U^A(x^A) + U^B(x^B - x^A) \tag{11}$$

In this equation, the small gravity term Mgx has been neglected with an error of the order $Mg/\hat{F}$. It is taken into account by including it in an effective U^{fall}. The net force at x^A has to be zero, that is $\frac{\partial U^A(x^A)}{\partial x^A} + \frac{\partial U^B(x^B - x^A)}{\partial x^B} = 0$. From this relation, one obtains the ratio x^A/x^B. Together with Eq. (11), an elementary calculation leads to Eq. (12)

$$\frac{U^A}{L^A} = \frac{U^{fall}}{L}\left(\frac{Q}{Q^A}\right)^{\frac{1}{m}} \tag{12}$$

in the limit $L^B \to L$. Thus, the weaker the contact zone, the more energy it has to absorb although the forces in both regions are equal. Eq. (12) determines the sequence of maximum deformations x_n^A (n=1, 2, …) as shown in Eq. (13)

$$\int_0^{x_n^A} P(x)F^m(x)dx = \hat{a}_m Q_n^A \int_0^{x_n^A}\left(\frac{x}{L^A}\right)^m dx + O(\mu) = U^{fall}\frac{L^A}{L}\left(\frac{Q}{Q_n^A}\right)^{\frac{1}{m}} + O(\mu) \tag{13}$$

with the cross-section independent parameter $\hat{a}_m$ which replaces a_m from section 1.
For the first fall n=1, the cross section of the contact zone is undamaged, that is $Q_1^A = Q$. The solution of Eq. (13) is given by Eq. (14)

$$\frac{x_n^A}{L_A} = \left(\frac{U^{fall}}{U}\right)^{\frac{1}{m+1}}\left(\frac{Q}{Q_n^A}\right)^{\frac{1}{m}} + O(\mu) \tag{14}$$

where the maximum elastic energy capacity $U = \hat{a}_m LQ/(m+1)$ of the new entire rope has been used. x_n^A, inserted in P(x) from Eq. (10), leads to a new cross section Q_{n+1}^A, which is smaller than the previous Q_n^A

$$\frac{Q_{n+1}^A}{Q_n^A} = e^{-\mu\left(\frac{x_n^A}{L^A}\right)^{m\lambda}} \cong 1 - \mu\left(\frac{x_n^A}{L^A}\right)^{m\lambda} + O(\mu^2) \tag{15}$$

exact in first order of μ. This accuracy is sufficient, because in the UIAA fall experiments several or even many falls are necessary for complete damage, implying a small damage per fall and thus a small μ. The integral over $P(x)F^m(x)$ in Eq. (13) can be evaluated exactly for the special case m=1 and λ=2 with the result from Eq. (15).
Inserting Eq. (14) in Eq. (15), a difference equation for Q_n^A follows as shown in Eq. (16)

$$\frac{Q_{n+1}^A}{Q_1^A} = \frac{Q_n^A}{Q_1^A} - \mu\left(\frac{U^{fall}}{U}\right)^{\frac{m\lambda}{m+1}}\left(\frac{Q_n^A}{Q_1^A}\right)^{1-\lambda} \tag{16}$$

 © 2018 Ulrich Leuthäusser

This equation cannot be solved analytically for arbitrary parameters λ. However, because μ is small, a continuous time solution is possible given by Eq. (17)

$$\frac{Q_n^A}{Q_1^A} = \frac{U_n^A}{U^A} \cong \left(1-\mu\lambda\left(\frac{U^{fall}}{U}\right)^{\frac{\lambda m}{m+1}}(n-1)\right)^{\frac{1}{\lambda}} \qquad \textbf{(17)}$$

Because the strain energy capacity U_n^A of the contact zone is proportional to Q_n^A at constant length L^A, Eq. (17) is also satisfied by U_n^A/U^A .

4. The fracture condition

The rope breaks in the nth fall when the fraction of the fall energy $U^A/L^A = \frac{U_{fall}}{L}\left(\frac{Q}{Q_n^A}\right)^{\frac{1}{m}}$

absorbed by the contact zone, exceeds the maximum storage energy $U_n^A = U\frac{Q_n^A L^A}{QL}$.

To take into account the damage by the plastic deformation, U has to be replaced by $U_{n+1}^e = U(1-\varepsilon_n^p)$ using either the solution ε_n^p from Eq. (7) or the approximate ε_n^p from Eq. (9). Thus, the fracture condition is shown in Eq. (18)

$$\left(\frac{Q_n^A}{Q}\right)^{\frac{m+1}{m}} = \frac{U^{fall}}{U_n^e} \qquad \textbf{(18)}$$

which has to be solved numerically. However, for most ropes which hold at least four falls, U_n^e can be replaced by its limit value U_∞^e because the process of plastic deformation is much faster than the local damage process.
Inserting Eq. (17) into Eq. (18) and solving for n, one obtains the critical number n* of falls which a rope can hold until it breaks (falls to failure minus one) as shown in Eq. (19)

$$n^* = \left\lceil \frac{1}{\mu\lambda}\left(\left(\frac{U_\infty^e}{U^{fall}}\right)^{\frac{m}{m+1}\lambda}-1\right)\right\rceil \qquad \textbf{(19)}$$

The ceiling brackets in Eq. (19) indicate that the right-hand side has to be rounded up so that for an energy U_∞^e , which is only an epsilon larger than U^{fall} , n*=1 results. For $\left(U_\infty^e/U^{fall}\right)^{\frac{m}{m+1}\lambda} >> 1$, i.e. for strong ropes, the scaling relation $n^*(U^{fall})/n^*(\alpha U^{fall}) = \alpha^{\frac{m}{m+1}\lambda}$ follows.

For the forces F^m, the relation between the force maximum $\hat{F}^m$ and n* is given by

$$\hat{F}^m = \frac{(F^m)^{max}}{(1+\mu\lambda n^*)^{1/\lambda}} \qquad \textbf{(20)}$$

Using Eq. (17) and assuming that there are different fall numbers $n_i < n_i^*$ of different fall energies U_i^{fall} with corresponding maximum forces $\hat{F}_i$, one can write for large n

$$1-\mu\lambda\left(\frac{U_1^{fall}}{U}\right)^{\frac{\lambda m}{m+1}} n_1 - \mu\lambda\left(\frac{U_2^{fall}}{U}\right)^{\frac{\lambda m}{m+1}} n_2 - \ldots \approx 0$$

From this relation the Palmgren-Miner[15] rule follows as shown below in Eq. (21)

$$1=\mu\lambda\sum_i n_i\left(\frac{\hat{F}_i}{F^{max}}\right)^{\lambda} = \sum_i \frac{n_i}{n_i^*} \quad \textbf{(21)}$$

Because the damage of the rope is described by probabilities P_n (Eq. (10)), the series of fall experiments has a stochastic component. Thus, the number of falls to failure n is a random variable with n* as the expectation value of n.
To calculate the fluctuations of n, a complicated first-passage time problem has to be solved. For P_n = constant, the standard deviation Σ(n) can be obtained from probability theory[16] given by Eq. (22)

$$\Sigma(n) = CV^{Wb}\sqrt{n^*} \quad \textbf{(22)}$$

where CV^{Wb} is the coefficient of variation for the Weibull distribution. This result can be understood by noticing that the standard deviation of a sum of n independent random variables is proportional to the square root of n.
For increasing n, the P_n decrease. This leads to a shorter damage process and therefore Eq. (22) overestimates the fluctuations on n.

σ·ω

5. Results and discussion of the experiments

The theoretical results of the previous sections are now compared with experimental data. First, the measured force-deformation curves of successive UIAA standard fall experiments[7] until fracture are shown in Fig. 3 for the rope Cobra 10.3.
The curves are convex, indicating nonlinear behaviour and the absence of friction because of adiabatic stretching. Furthermore, Fig. 3 shows that the force maxima reach a final value after some falls and the spring constant k as the initial slope of the force-elongation curves increases with increasing fall number, i.e. the rope gets stiffer.

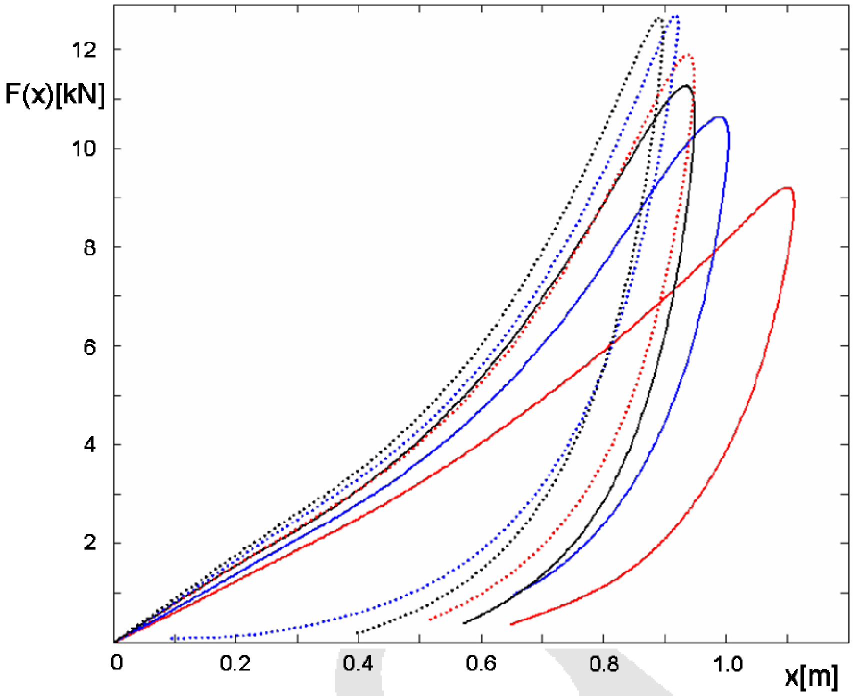

Figure 3. Force-deformation curves of the UIAA fall experiment for Cobra 10.3 until rope fracture. Shown are the falls 1(red), 2(blue), 3(black), 4(red dots), 6(blue dots), 8(black dots). Falls 5 and 7 are omitted for clarity. Fracture occurs in the 9th fall.

With the force equation $F(x/L_e)$ from Eq. (1), all force-deformation curves of Fig. 3 can approximately be mapped to a single curve by scaling the deformation x with the appropriate elastic maximum deformation L_n^e depending on the fall number n.
The result is shown in Fig. 4, where the curves in bold are the scaled Cobra curves from Fig. 3. The calculated $F(x/L_e)$ from Eq. (1) is represented by the dotted black curve. For a second rope, the Joker 9.1 which is very different than the Cobra, the same scaling procedure has been applied. It is represented by the set of curves to the right of the Cobra curves also with the calculated $F(x/L_e)$ in black dots.
The success of the scaling procedure is another indication for delayed friction during the first part of the motion, because a velocity dependent friction term in Eq. (3) would destroy this scaling behaviour.

 © 2018 Ulrich Leuthäusser

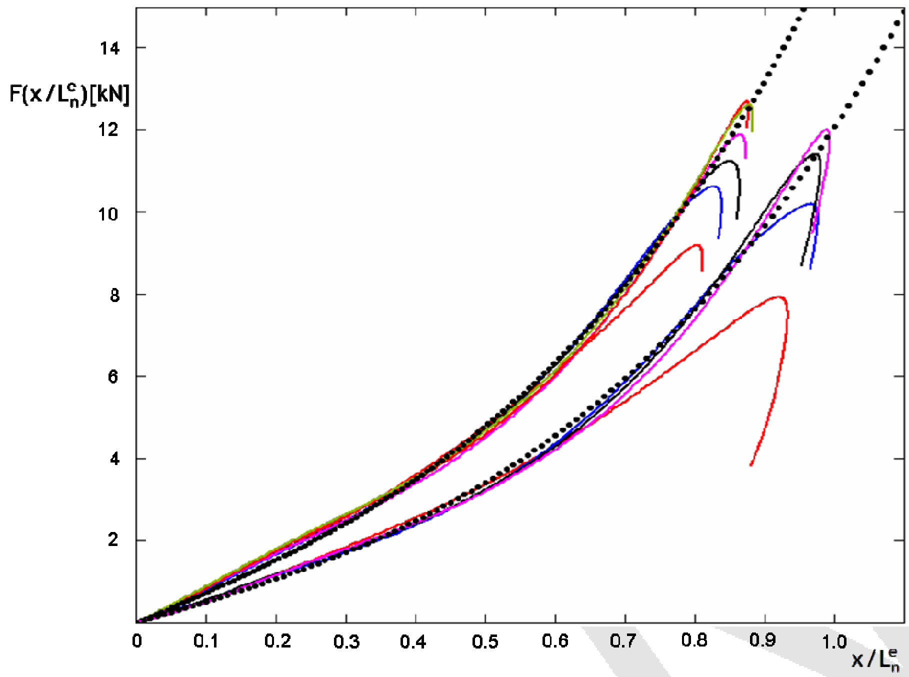

Figure 4. Scaling of the force-deformation curves with L_n^e for the Cobra rope (left set of curves) and for the Joker rope to the right. All curves from Fig. 3 coincide with $F(z)=a_1z+a_3z^3$ with $z=x/L_n^e$.

In Fig. 5, the sequence of the elastic maxima L_n^e (black dots) for the Cobra rope, obtained from the above scaling procedure, is shown. In a fast process of a few falls, the rope loses approximately 30% of its initial energy storage capacity. The $L_{n+1}^e/L_1^e = 1-\varepsilon_n^p$ obtained by the iteration of the plastic flow Eq. (7) for ε_n^p are shown in Fig. 5 as a red line. For the fit, a yield stress of about 45% of the fracture stress σ^{max} has to be used. This value is in agreement with the yield stress values for nylon found in literature.

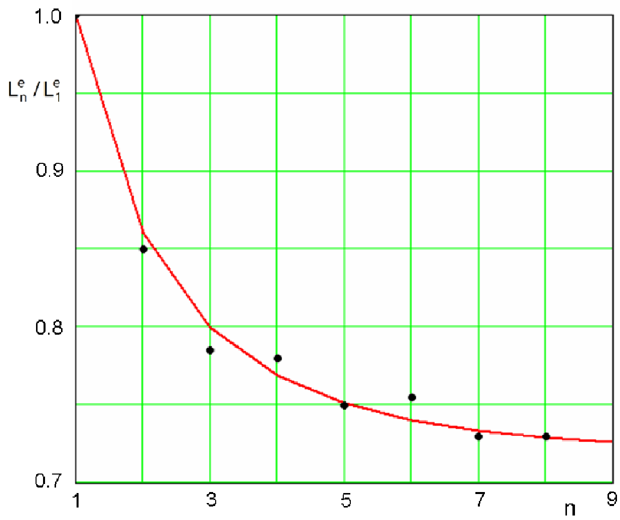

Figure 5. Maximum elastic deformations L_n^e from Eqs. (6) and (7) as a function of the fall number n. Major changes in the internal structure of the rope occur in the first few falls with the greatest loss of its elastic properties.

 © 2018 Ulrich Leuthäusser

Furthermore, the decreasing L_n^e are responsible for the increase of approximately 40% of the spring constants $k_n \propto 1/L_n^e$ before they reach their final value (Fig. 3).
Table 1 shows the values of the elastic moduli a_1 and a_3 for the Cobra and Joker rope and other characteristic values, together with their relative differences.

	D[mm]	Q[m²]	a_1[kN]	a_3[kN]	a_3/a_1	L_1^e[m]	L[m]	L_1^e/L
Cobra 10.3	10.3	8.33E-05	7.3	9.1	1.25	1.38	2.6	0.531
Joker 9.1	9.1	6.50E-05	5.2	7.0	1.35	1.39	2.6	0.535
rel. diff.	13%	28%	40%	30%	-7%	-1%	0%	-1%
	F^{max}[kN]	U[kJ]	u[kJ/m³]	U/U^{fall}	σ^{max}[MPa]	σ^y[MPa]	F^y/F^{max}	n*
Cobra 10.3	16.4	8.19	3.78E+04	1.90	197	89	0.45	8
Joker 9.1	12.2	6.08	3.60E+04	1.41	188	83	0.44	4
rel. diff.	34%	35%	5%	35%	5%	7%	2%	100%

Table 1. The total energy storage capacity of the new rope is determined by $U = 1/2\, L_1^e (a_1 + a_3/2)$. For the Cobra 10.3, one obtains U =1.9U^{fall} with eight successfully held falls. In contrast, the Joker 9.1 has a U = 1.4U^{fall} and only four successful falls. Note that the energy density u = U/QL, the maximum possible elastic deformation L_1^e, the maximum stress σ^{max} and yield stress σ^y of the two ropes differ only slightly, which justifies the assumption that these values are mainly material dependent.

From the relative differences in Table 1, both ropes have approximately the same maximum strain energy storage density u, ultimate stress σ^{max} and yield stress σ^y, although their spring constants are very different. This is a strong indication for the assumption that mainly the cross section determines the energy storage capacity at a fixed rope length.

The mean number of falls to failure n* and the cross section of climbing ropes have to be published by the rope manufacturers. A representative selection[17] of climbing ropes has been chosen for the plot n* vs. U^{fall}/U for comparison with the numerical solution of Eq. (18). The result is shown in Fig. 6.
The red curve shows the number of falls to failure in dependence of U^{fall}/U, when only local damage is present. For $U^{fall}/U \geq 0.4$ and n* ≤ 20, the data points deviate from the red curve and follow the black curve below the red one. In the black curve, the contribution of plastic deformation is added to the local damage effect and thus the number of falls to failure is approximately reduced by 25% for $U^{fall}/U \approx 0.5$.
Because of the probabilistic nature of the damage process, the data scatter around their mean value n*. In Fig. 6, the blue dotted lines represent the fluctuation intervals $n^* \pm \Sigma(n^*)$ with the standard deviation Σ(n*) from Eq. (22). Published variations[18] of n for n*~10 match with Σ(n*)~1-2.
Note that there are additional sources of data scattering. The theory presented does not take into account the varying damage parameter μ that depends on differing surface coating, the mantle/kernel ratio which varies a few percent, and measurement errors in the data of the manufacturers.

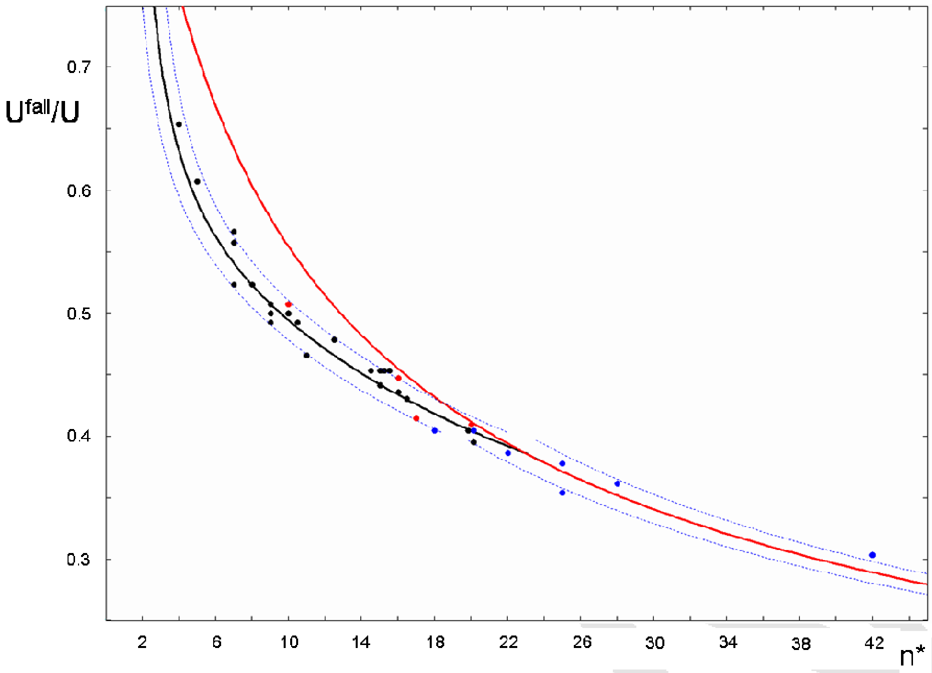

Figure 6. U^{fall} vs. number of falls to failure n* in analogy to the stress-cycle curves used in materials science. The Weibull parameter is given by λ=2.5 from which a CV^{Wb} = 0.4 follows. The damage parameter is μ=0.09. The black dots are from single ropes, the blue dots from twin ropes and the red dots from half ropes (tested with only 69% of the single rope's fall energy). The position of the transition point is at $U^{fall}/U \approx 0.4$ and n* ≈ 20. All ropes with lower n* are plastically deformed.

Conclusion

In this paper, a theoretical model has been presented which describes two mechanisms for the fracture of a climbing rope.
The first mechanism, homogeneous plastic deformation, has been treated as a Bingham plasticity model with a nonlinear force derived from statistical mechanics. Plastic deformation leads to a successive shortening of the maximum elastic elongation and thus reduces the elastic storage capacity of the rope. For UIAA standard falls, the reduction is approximately 30% of the initial capacity.
Experimentally, plastic deformation becomes noticeable by an increasing spring constant k of the rope. Using the changes of k, the experimental force-elongation curves for all falls from the first fall until failure can be explained by scaling them to one underlying nonlinear force.

Although plastic deformation weakens the rope, it is usually not sufficient to explain fracture and a second mechanism is necessary. This mechanism is the large local stress wearing down the cross section of the rope in the contact zone rope/anchor. It has been phenomenologically described by a probabilistic model using a Weibull failure probability, resulting in a difference equation for the successive damage of the contact zone.
The question, why ropes damaged from fall experiments get stiffer although the reduction of the rope's cross section by abrasion should soften them, can now be answered: local damage leads only to a small reduction of the spring constant proportional to the short length of the contact zone. Plastic deformation affecting the whole rope, however, reduces the elastic stretchability and leads in total to a larger spring constant.

Both mechanisms have been combined for the calculation of the mean number n* of falls to failure which is mainly a function of the ratio between fall energy and energy storage capacity. A quantitative agreement of the calculated n* with the measured falls to failure for many ropes has been achieved. Also the calculated variations of n as a consequence of the underlying probabilistic model agree with the experimentally detected fluctuations.

To summarize, the presented theory is able to explain the changing dynamic behaviour of a climbing rope in the course of the fall experiments, as well as to determine the number of falls until the rope breaks.

 © 2018 Ulrich Leuthäusser

References

[1]Runesson K. Constitutive Modeling of Engineering Materials – Theory and Computation. http://www.am.chalmers.se/~ragnar/material_mechanics_home/literature/ThePrimer_(1).pdf

[2] Roylance D. Mechanical Properties of Materials. http://web.mit.edu/course/3/3.225/book.pdf

[3] Alava MJ. et al. Statistical Models of Fracture. https://arxiv.org/abs/cond-mat/0609650

[4] Pavier M. Experimental and theoretical simulations of climbing falls. Sport Eng. 1998, 1: 79-91.

[5] Pradhari S. et al. Failure Processes in Elastic Fiber Bundles. https://arxiv.org/abs/0808.1375

[6] http://www.theuiaa.org/safety-standards/#standards1

[7] UIAA norm fall tests for climbing ropes. IFT University of Stuttgart 2012

[8] http://www.engineersedge.com/material_science/yield_strength.htm

[9] Rubinstein M., Colby RH. Polymer Physics. Oxford University Press

[10] Newman SB., Wheeler HG. Impact Strength of Nylon and of Sisal Ropes. Journal of Research of the National Bureau of Standards, Volume 35, 417-431

[11] Leuthäusser U. The physics of a climbing rope under a heavy dynamic load. Proceedings of the Institution of Mechanical Engineers, Part P: Journal of Sports Engineering and Technology. Vol. 231, Issue 2 (2017)

[12] Lubliner J. Plasticity Theory. Dover Publications (2008)

[13] Poston T. Stewart I. Catastrophe Theory and its Applications. Pitman, San Francisco (1978)

[14] Popov V. Rigorous Treatment of Contact Problems – Hertzian Contact. In: Contact Mechanics and Friction. Springer, Berlin, Heidelberg (2017)

[15] Fatemi A., Yang L. Cumulative fatigue damage and life prediction theories: a survey of the state of the art for homogeneous materials. Int. J. Fatigue Vo. 20, No. 1, pp. 9-34 (1998)

[16] Feller, W. An Introduction to Probability Theory and its Applications. Chapter 14, pp.348. J. Wiley & Sons (1968)

[17] Used ropes: Tendon (www.mytendon.com) Ambition, Trust, Master. Edelweiß (www.edelweiss-ropes.com) Element, Power, Oflex. Edelrid (www.edelrid.de) Power, Cobra, Tower. Mammut (www.mammut.com) Gravity, Serenity. Beal (www.beal-planet.com) Joker, Apollo, Opera. Bornack (www.bornack.de) 11.4. Maxim (www.maximropes.com) Glider, Pinnacle. Bluewater (www.bluewaterropes.com) Enduro. Petzl (www.petzl.com) Tango, Contact, Paso, Salsa, Rumba.

[18] http://www.mytendon.com/

COPY